Volume 1 | Number 1 | Jan 2013 | Pages 1–100

Journal of
Materials Chemistry A

Materials for energy and sustainability
www.rsc.org/materialsA

ROYAL SOCIETY
OF CHEMISTRY

How dose the Silicon Element Perform in JD-dyes: A Theoretical Investigation

Li-Na Yang,[a] Shi-Lu Chen,*[a] and Ze-Sheng Li*[a]

[a]*Key Laboratory of Cluster Science of Ministry of Education, Beijing Key Laboratory of Photoelectronic/Electrophotonic Conversion Materials, Beijing Key Laboratory for Chemical Power Source and Green Catalysis, School of Chemistry, Beijing Institute of Technology, Beijing 100081, China*

Tel: +86 01 6891 8670;

E-mail: shlchen@bit.edu.cn (S.-L. Chen), zeshengli@bit.edu.cn (Z.-S. Li)

1

ABSTRACT

Inspired by the successful utilization of silicon cores axially coordinated by trihexylsiloxy groups in naphthalo/phthalocyanine dyes, using ullazine-based dye JD21 as the prototype, we designed three novel silicon-core JD analogues in this paper. Based on the theoretical analysis on the four dyes and the corresponding dye/$(TiO_2)_{38}$ complexes, the Y2 dye with the dithienosilole (DTS) conjugation unit is recognized as a star molecule, for its impressive performance in various aspects, including remarkable light-harvesting capability, large driving force for dye regeneration (ΔG_{reg} = 0.65 eV), excellent balance between the rates of electron injection (k_{inj} = 1.48$\times10^{12}$ s^{-1}) and electron-hole recombination (k_{rec} = 1.68$\times10^{10}$ s^{-1}), and high stability for the adsorbed system of Y2/$(TiO_2)_{38}$. It is thus proposed to be a promising candidate to be applied in dye-sensitized solar cells (DSCs).

Keywords

Dye-sensitized solar cell; Ullazine group; Light-harvesting capability; Thermodynamic property; Kinetic parameter; Long-term stability

1. Introduction

Dye-sensitized solar cells (DSCs) have attracted continuous attention[1-3] since the pioneering work by Grätzel *et al.* in 1991.[4] One of the most vital components in DSCs is assigned to dye molecules, which are responsible for light harvesting and electron injection at dye/semiconductor interface. To improve the power conversion efficiency (PCE) of DSCs, the current researches about dye molecules mainly focus on two aspects. One is metal-organic dyes, such as the state-of-the-art zinc-porphyrin dyes[5, 6] and Ru(II) polypyridyl dyes.[7, 8] Quite recently, the solar cell devised with a benzothiadiazole (BTD)-based zinc-porphyrin dye (SM315) has been reported to achieve the record PCE of 13% without any co-sensitizer.[9] The other is the organic molecules featured with the donor-π-linker-acceptor (D-π-A) structure.[10-12] Recently, an efficiency of 10.65% has been attained by the YA422-sensitized solar cell, indicating the significant influence of donor size on dye performance.[13] It is also shown that the properties of dyes are affected by the nature of π-conjugation units[14] as well as the acceptor moiety.[15, 16] For example, by forming the firm Si–O–Ti (titanosiloxane) bonds between dyes and the TiO_2 substrate, organosilicon compounds such as ADEKA-1 show their charming potential in DSC applications.[17, 18]

The nitrogen-containing heterocycle (ullazine group) with 16-π electrons is a promising unit in DSCs due to its strong intramolecular charge transfer. The ullazine-based dyes (denoted as JD-dyes) were first synthesized and used as optoelectronic materials in DSCs by Grätzel *et al.* in 2013.[19] Among their tested

devices, the solar cell sensitized by a low-molecular-weight (MW) JD21 dye shows a remarkable photovoltaic performance (MW = 638 g mol^{-1}, PCE = 8.4 %). Since that, a few theoretical investigations on JD-dyes were carried out by Meng *et al.*[20, 21] to explore potentially efficient sensitizers for DSCs. However, the relatively planar geometry of the ullazine group in JD-dyes may increase the unfavorable dye aggregation on semiconductor surface, and consequently hinder their further applications in DSCs. In this paper, inspired by the successful utilization of silicon cores axially coordinated by trihexylsiloxy groups in naphthalo/phthalocyanine dyes,[22, 23] we designed a series of silicon-core JD analogues based on the JD21 backbone, by introducing three classic π-conjugation units (cyclopentadithiophene (CPDT),[24, 25] dithienosilole (DTS),[26] and dithienopyrrole (DTP)[25, 27]) between ullazine and cyanoacrylic acid groups. The newly engineered dyes were named by Y1, Y2, and Y3, respectively (see Scheme 1). Systematic investigations show that the DTS-containing Y2 dye displays remarkable light-harvesting capability, favorable thermodynamic properties, good kinetic parameters, and high stability for the adsorbed system of Y2/(TiO$_2$)$_{38}$. It is thus proposed to be a potential dye toward more efficient DSCs.

JD21   X = -C(CH$_3$)$_2$(Y1), -Si(CH$_3$)$_2$(Y2), -NCH$_3$(Y3)
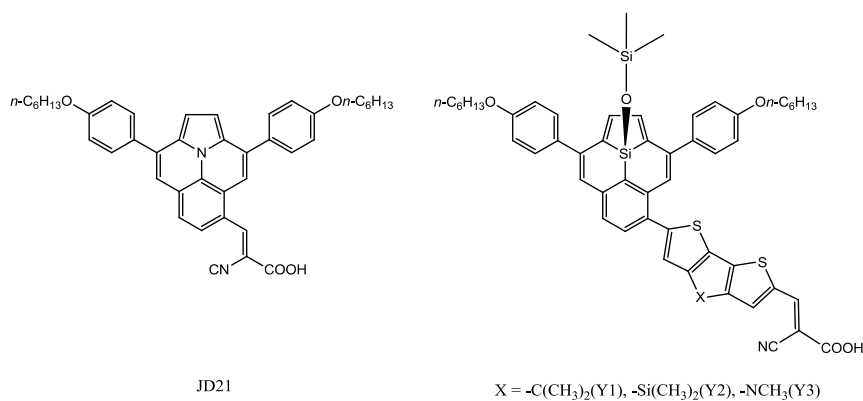
Scheme 1. Chemical structures of the dyes investigated in this paper.

2. Computational details

The geometric optimizations of the ground-state dyes were carried out by the density functional theory (DFT) B3LYP functional[28] coupled with a 6-31G(d,p) basis set in the dichloromethane (CH_2Cl_2) solution. Bulk solvent effects of CH_2Cl_2 were included by means of the conducting polarizable continuum model (C-PCM).[29] Frequency analysis was then performed to confirm the nature of all structures at the same theory level as geometric optimizations. Based on the optimized geometries, optical properties were obtained by calculating the vertical transitions of the lowest 50 singlet-singlet excited states in the CH_2Cl_2 solution using time-dependent DFT (TD-DFT) with the coulomb-attenuating method (CAM-B3LYP)[30] and the 6-31G(d,p) basis set.

To obtain the excited-state (ESOP) and ground-state oxidation potentials (GSOP, also termed by ΔG_{ox}), two values reflecting the driving forces for electron injection and dye regeneration respectively, geometric optimizations of dyes in their excited, oxidized, and ground states were done in the CH_2Cl_2 solution by the CAM-B3LYP/6-31+G(d,p) method (the related details have been discussed in our previous paper about squaraine dyes[31]). All calculations mentioned above were implemented in the Gaussian 09 program package.[32]

The electronic coupling between dyes and the semiconductor (anatase) surface through anchoring groups were also investigated. As known, the (101), (001), and

(100) facets are the three most frequently exposed facets in natural anatase samples.[33] Among these three facets, the most stable (101) facet is observed to dominate the anatase crystal surface (more than 94% exposed surface is constituted by the $TiO_2(101)$ facet).[34, 35] Therefore, the current study of dye adsorption on anatase will focus on the $TiO_2(101)$ surface. In the present case, a $(TiO_2)_{38}$ cluster, which was obtained by cutting an anatase slab with the (101) surface exposed, was used to simulate the TiO_2 nanoparticle. Here, dye/$(TiO_2)_{38}$ complexes were optimized using spin-unrestricted DFT with the PBE functional[36, 37] and double-numeric quality basis set with polarization functions (DNP) in the CH_2Cl_2 solution, where the solvation effects were considered by the conductor-like screening model (COSMO).[38] These calculations were carried out by the DMol[3] package in Material studio.[39, 40] The convergence criterions for energy, force, and displacement were 2×10^{-5} Ha, 4×10^{-3} Ha/Å and 5×10^{-3} Å, respectively, with a Fermi smearing of 0.005 hartree (1 Ha = 27.2114 eV) and a global orbital cutoff of 4.5 Å. Based on the DMol[3]-optimized dye/$(TiO_2)_{38}$ complexes, single-point DFT and TD-DFT calculations in the CH_2Cl_2 solution were performed in Gaussian 09 to obtain electronic and optical properties of adsorbed dyes at the same theory level as that for isolated dyes.
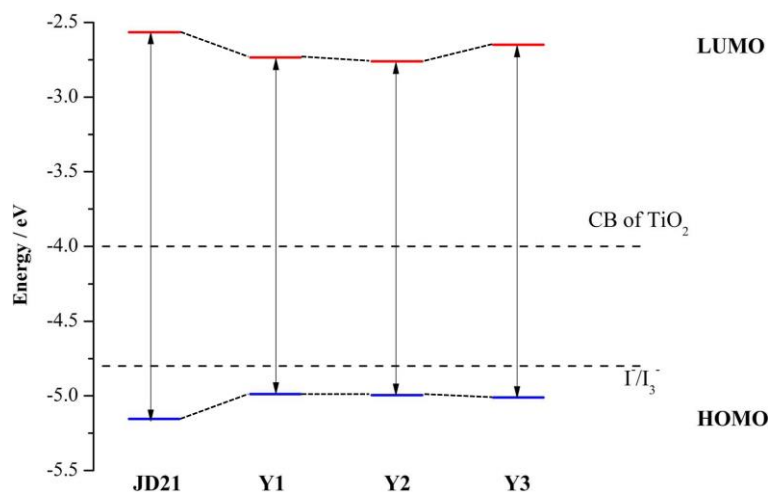
Figure 1. Energy-level arrangements of the investigated dyes together with the experimental conduction band edge of TiO_2 and the redox potential of I^-/I_3^-.

3. Results and discussion

3.1 Structures and properties of JD-dyes

With the aid of DFT and TD-DFT approaches, it is able to scrutinize dyes from their energy levels and light-harvesting capabilities. It is a common experience that a dye should be ruled out as a sensitizer in DSCs when its highest occupied molecular orbital (HOMO) is energetically higher than the redox potential of the electrolyte (I^-/I_3^-), its lowest unoccupied molecular orbital (LUMO) level is under the conduction band (CB) edge of semiconductor (commonly TiO_2), or it is of worse optical properties. With this, the electronic and optical properties of the investigated dyes were calculated. As shown in Figure 1, all dyes exhibit appropriate HOMO/LUMO energy levels, which insure a fast and unidirectional electron transfer process. In addition, all newly designed dyes display additional absorption bands around 400 nm compared with the original JD21 dye (Figures 2 and S1), although slight blue shifts at

the maximum absorption (λ_{max}) were observed. The absorption around 400 nm for newly-designed dyes fills well in the absorption dip in the light-harvesting efficiency (LHE) curve as the case of JD21 (Figure S2, see the Supplementary Information for the details about the LHE curve). In particular, the designed silicon-core dye with DTS as the π-conjugation bridge (Y2) has an absorption almost spreading from 300-600 nm, showing a good capability in light harvesting. Therefore, a DSC sensitized by the Y2 dye is expected to attain a comparable short-circuit photocurrent (J_{SC}) potential to that by JD21. The properties upon photo-excitation are summarized in Table 1, and the main frontier molecular orbitals responsible for the λ_{max} of dyes are given in Figure S3. It can be found from Table 1 that the transition from HOMO to LUMO is the most important contribution to the λ_{max} of all dyes. The HOMOs of all dyes almost delocalize over the whole dye molecules with a larger proportion on ullazine/ullazine-like group, while the LUMOs are localized mostly at the π-conjugation units and acceptor part (Figure S3). This implies the good capability of charge separation upon photo-excitation.
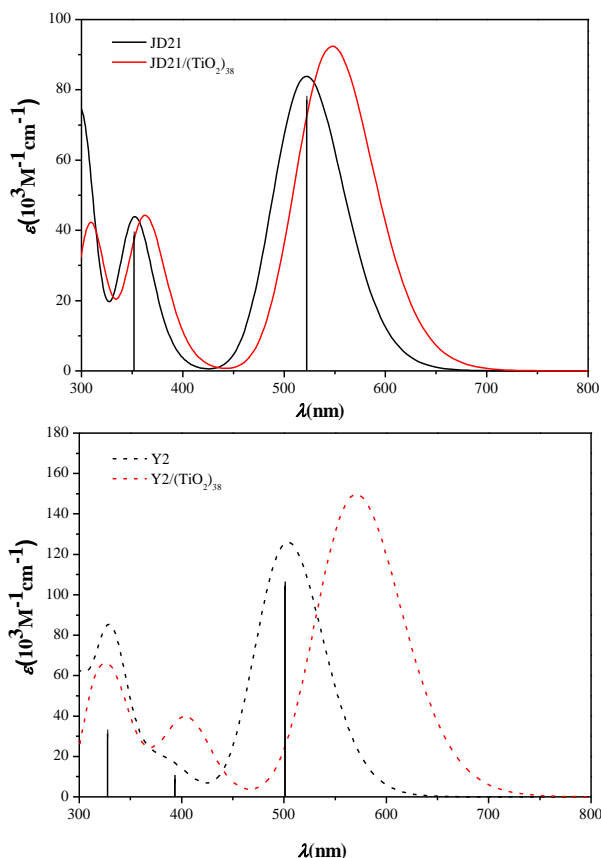
Figure 2. The absorption spectra for isolated JD21 (black solid line), JD21/(TiO$_2$)$_{38}$ complex (red solid line), isolated Y2 (black dash line), and Y2/(TiO$_2$)$_{38}$ complex (red dash line) dissolved in the CH$_2$Cl$_2$ solution.

3.2 Dyes adsorbed on the TiO$_2$ surface

3.2.1 Electronic and optical properties of dye/(TiO$_2$)$_{38}$ complexes

It is well-known that the efficiency of electron injection is strongly dependent on the electronic coupling between dye and the semiconductor surface. It was reported by Meng *et al.* that a tridentate-bridging (TB) mode, where one interface O-Ti bond, one N-Ti bond, and an additional hydrogen bond between the anchor group and TiO$_2$ are formed, is more stable in energy for the adsorbed dye than the bidentate-bridging (BB)

9

configuration.[20, 21] In the present work, many attempts have been made to find such a stable TB configuration but failed. Therefore, the dye/$(TiO_2)_{38}$ complexes with the BB configurations were employed in the following investigations.

Using the same computational procedure as free dyes, we obtained the UV-Vis spectra of dye/$(TiO_2)_{38}$ complexes. It is demonstrated that all adsorbed dyes show red-shifted absorption spectra compared to the corresponding free dyes (Figures 2 and S1). For the Y-dye/$(TiO_2)_{38}$ complexes, the amounts of red-shift at λ_{max} are larger (ca. 60 nm) than that of the JD21/$(TiO_2)_{38}$ complex (30 nm). As seen in Figure S2, the adsorbed JD21 present a similar dip in the LHE curve to that in isolated state. Relative to the bound JD21, the Y1/$(TiO_2)_{38}$ and Y2/$(TiO_2)_{38}$ complexes harvest light in higher efficiency with broader spectral response (the LHEs almost reach 100% in the range of 300-750 nm). The analysis of the most important single-particle excitations reveals that the HOMOs of dye/$(TiO_2)_{38}$ complexes delocalize over whole dye molecules, while the LUMOs mainly localize on the TiO_2 nanoparticle (Figures 3 and S4). Such an orbital distribution is beneficial to the charge transfer at dye/semiconductor interface, and is essential for constructing a cell with high electron-injection efficiency.
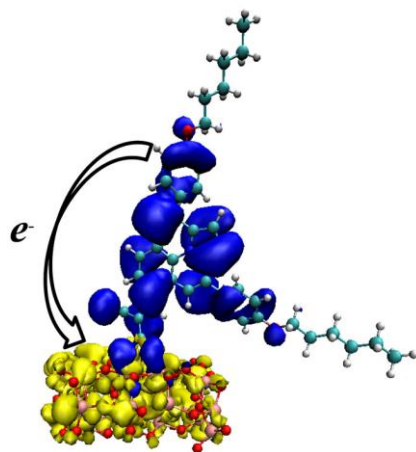
Figure 3. The molecular orbital distribution of JD21/(TiO$_2$)$_{38}$ complex in the CH$_2$Cl$_2$

solution. Blue and yellow indicate HOMO and LUMO electronic density, respectively.

The arrow represents the direction of charge transfer.

3.2.2 The shift of the conduction band edge

Besides the broad spectral response, a potential cell should also possess a high

open-circuit photovoltage (V_{oc}) value. The V_{oc} of a DSC is directly relevant with the

conduction band (CB) edge (E_{CB}) of semiconductor. As stated by De Angelis and his

coworkers, the adsorption of dye molecules on TiO$_2$ surface can induce a shift of the

conduction band profile of TiO$_2$ (ΔE_{CB}).[41] In order to evaluate the ΔE_{CB} of TiO$_2$ in our

systems, the total densities of states (TDOS) for bare TiO$_2$ and the projected densities

of states (PDOS) for TiO$_2$ in dye/(TiO$_2$)$_{38}$ complexes were calculated. The related

curves were plotted using a Gaussian function. A linear fit of the low energies profile

in a range from 20% - 80% of the maximum height was subsequently performed and

the intercept of this line with the energy axis was taken as E_{CB} (Figures 4 and S5). The

detailed results have been summarized in Table 2. It can be seen that the adsorption of

a dye on TiO_2 surface results in an upshift of CB edge. The amount of CB shift (ΔE_{CB}) of JD21 (0.061 eV) is larger than those of Y-dyes (~ 0.04 eV). It was also demonstrated by De Angelis *et al.* that the effects of a dye on ΔE_{CB} can be divided into two aspects, namely, charge transfer (CT) and electrostatic (EL) effects.[41] The occurrence and extent of CT at dye-titanium interface can be examined through the isodensity contour plots of electron density difference and the charge displacement (CD) analysis.[42] In the dye/$(TiO_2)_{38}$ adsorbed systems (Figures 5 and S6), an evident rearrangement of electron density can be observed in both dye and semiconductor surface compared to the isolated fragments. In particular, the significant depletion of electron density happens around the cyanoacrylic acid group, and electron density accumulates mainly at the dye-TiO_2 interface, which can be quantitatively characterized by the CD curve (Figures 5 and S6). Among all investigated complexes, the minimum CT was observed in the Y1/$(TiO_2)_{38}$ system (0.37 e^-), indicating a weaker interaction between Y1 and TiO_2 (Table 2). The EL (primarily due to the dye dipole) contribution to ΔE_{CB} can be obtained by the analysis of the average dye electrostatic potential on TiO_2 surface (V_{EL}). It was found that the calculated V_{EL} values of all Y-dyes (-6.0 eV) are much larger than that of JD21 (-0.7 eV) (Table 2). With these results, it can be concluded that, upon dye adsorption onto TiO_2 surface, the charge transfer from a dye to TiO_2 surface shows a larger contribution to ΔE_{CB} compared to the electrostatic potential (see the Supplementary Information for the details about the CD curve and V_{EL} analysis).
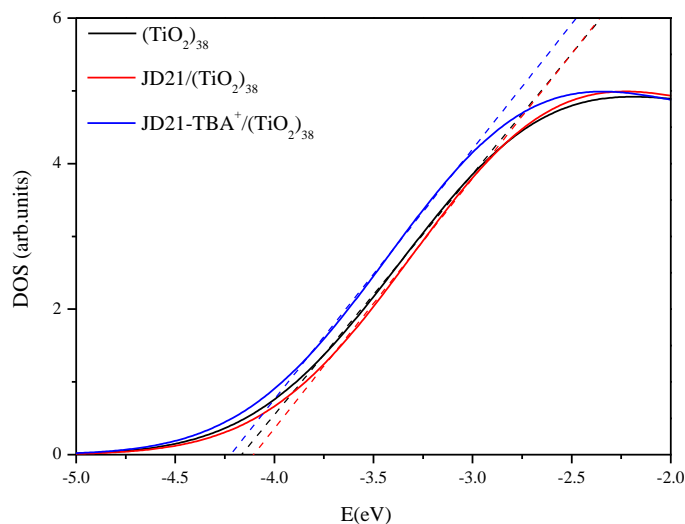
Figure 4. Total (DOS) and partial density of states (PDOS) for JD21 adsorbed onto a

$(TiO_2)_{38}$ cluster. Black solid line: $(TiO_2)_{38}$ cluster DOS. Red solid line: $(TiO_2)_{38}$ cluster

PDOS with dye adsorbed. Blue solid line: $(TiO_2)_{38}$ cluster PDOS with dye-TBA$^+$

co-adsorbed. The intercepts of dash lines with the energy axis correspond to the

calculated CB edges.

To enhance the performance of a DSC device, a suitable amount of cations (one or

several kinds of cations with a certain ratio) are often involved in the electrolyte, to be

utilized to regulate the CB position of the semiconductor[43] and the electron-injection

efficiency of the excited dye.[44, 45] In this paper, the influence of such ions on CB shift

has been examined by modeling the dye/cation co-adsorbed systems, where a

commonly-used cationic species named tetra-*n*-butylammonium ion (TBA$^+$) is

adsorbed on the surface of a $(TiO_2)_{38}$ cluster together with the investigated dyes.

To optimize the JD21-TBA$^+$ and Y1-TBA$^+$ adducts, four initial conformations were

employed by keeping the TBA$^+$ cation close to the electron-rich moieties of dye

molecules. The geometries of these conformers optimized in the dichloromethane

13

solution are given in Figures S7 and S8, along with their relative energies. In the lowest-energy configuration of JD21-TBA$^+$ adduct (Conf. 3), the TBA$^+$ cationic ion is located near the in-plane nitrogen of the ullazine group, whereas, the conformer with TBA$^+$ close to the cyanoacrylic acid group is the most stable for Y1-TBA$^+$ adduct (Conf. 4). The corresponding binding energy of each most stable configuration was also computed, which is defined as the difference between the energy of the adduct and the energy sum of the isolated fragments.[46] Thus positive/negative values indicate destabilization/stabilization of the dye-TBA$^+$ adduct compared to the isolated species. Here, the negative binding energies between JD21/Y1 and TBA$^+$ (-0.86 eV and -0.78 eV, respectively, see Table 2) clearly suggest the tendency to form stable dye-TBA$^+$ adducts in solutions.

With the stable geometries of dye-TBA$^+$ adducts, the geometric optimizations of dye-TBA$^+$ co-adsorbed systems were performed (Figure S9). Our calculations show that the co-adsorption results in a downshift of the CB edge ca. 0.1 eV compared with the mono-adsorption of dye molecules (Figures 4 and S5), which may decrease the V_{oc} of a cell and reduce the efficiency of electron injection from an excited dye to TiO$_2$. Therefore, an overall consideration should be made in the fabrication of a cell.
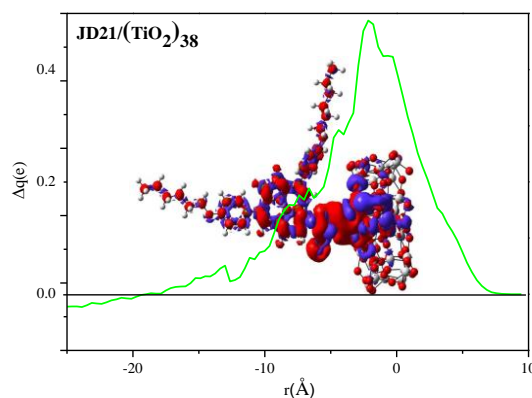
Figure 5. Isodensity contour plot and charge displacement curve for JD21 adsorbed onto TiO_2 in BB configuration. The red surface identifies the region in which the electron density decreases. The zone of density accumulation is marked by blue.

3.2.3 The thermodynamic and kinetic properties of dye/$(TiO_2)_{38}$ complexes

Due to the direct relevance of ESOP to the electron injection and of GSOP to the regeneration of an oxidized dye, the two values of ESOP and GSOP become crucial. The energy difference between ESOP and the CB edge of TiO_2 is the driving force for the electron injection (ΔG_{inj}) from an excited-state dye to semiconductor, while the energy difference between GSOP and the oxidation potential of redox couple means the driving force for the regeneration of an oxidized dye (ΔG_{reg}). It has been known that a typical driving force required for electron injection is usually on the order of tenth eV, while the one for the regeneration of an oxidized dye should be at least 0.4 eV with the I^-/I_3^- redox shuttle.[22] Keeping this in mind, the ESOP and GSOP of the studied dyes have been computed using the previously reported procedure which has been successfully applied to both Ru(II) polypyridyl and several organic dyes.[31, 47] The obtained ESOP, GSOP, and driving forces for electron injection (ΔG_{inj}) and dye regeneration (ΔG_{reg}) are summarized in Table 3. One can find in Table 3 that the ESOP values for all investigated dyes are obviously higher in energy than the CB edge of titanium, thus suggesting a thermodynamically favorable injection of the first excited electron from the adsorbate to the substrate (the ΔG_{inj} of the investigated dyes is in the range of 1.1 - 1.9 eV). It can further be found that Y1 and Y2 show the

cathodic shift of ESOP relative to JD21, which leads to the smaller ΔG_{inj} for Y1 and

Y2 (~ 1.1 eV). Though the ΔG_{inj} of Y1 and Y2 are smaller, it is sufficient for Y1 and

Y2 to effectively inject electrons to TiO_2. On the other hand, for all investigated dyes,

the amount of the lowering of GSOP compared to the redox potential of I^-/I_3^- are

satisfying for the regeneration of oxidized dyes (Table 3). In particular, for Y-dyes, the

significant downshifts of GSOP ~ 0.2 eV compared to that of JD21 finally result in

larger driving forces for the regenerations of oxidized Y-dyes (ΔG_{reg} of Y-dyes are ca.
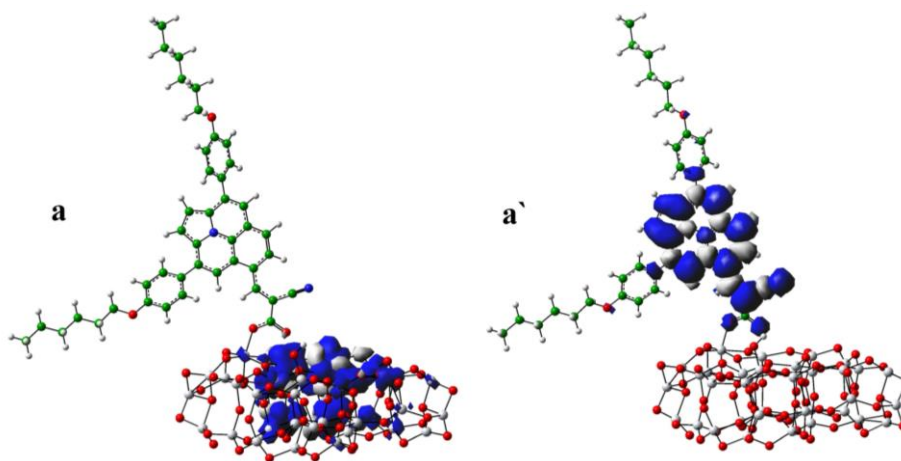
0.6 eV).

Figure 6. Spin densities for the reduced (a) and oxidized (a`) JD21/$(TiO_2)_{38}$

complexes.

Another simplified, but informative, way to assess the efficiencies of electron

injection and dye regeneration is to analyze the spin density distributions in the

corresponding one-electron-reduced and one-electron-oxidized species (see Figures 6

and S10). Such an approach has been successfully applied to several systems

including pyridinium-based and ruthenium polypyridyl dyes.[44, 48-50] It appears that the

spin densities of all reduced dye/$(TiO_2)_{38}$ complexes almost entirely localize on the

TiO_2 substrate, as a result of the sufficient driving forces for electron injection.

However, it seems quite different in oxidized complexes. The holes of all oxidized

dye/$(TiO_2)_{38}$ complexes are delocalized over the whole dye molecules with larger

proportions on the ullazine/ullazine-like groups. It is further found that the two

benzenes at the periphery of ullazine-like group in Y-dye/$(TiO_2)_{38}$ complexes show a

larger spin distribution, compared to that in JD21 complex. The more distributions of

holes in the donor moieties of Y-dyes can enhance the interactions between the

oxidized Y-dyes and the I^-/I_3^- redox couple. These strong interactions, together with

the larger ΔG_{reg} values for oxidized Y-dyes, may eventually lead to a faster

regeneration of Y-dyes, compared to the oxidized JD21.

It has been revealed above that, in JD21 and Y-dyes, the HOMO is mainly localized

at the ullazine/ullazine-like heterocycle, while the LUMO primarily locates at the

cyanoacrylic acid group (Figure S3). Upon irradiation, one electron is excited from

HOMO to LUMO, and is subsequently injected to the CB of TiO_2. Thus, the distance

between the dye anchor and the TiO_2 surface (Figure S11) can be defined as the

distance of electron injection (r_{inj}). With this, the r_{inj} values for all dyes are obtained

(all of them are about 2.0 Å, summarized in Table 3). On the other hand, the injected

electron may be transferred back from the CB of TiO_2 to the HOMO orbital of the dye,

which is the electron-hole recombination process. The distance of recombination (r_{rec})

can be roughly estimated from the distance between the donor center of the dye (the

silicon atom in the present case) and the TiO_2 surface (Figure S11). The obtained r_{rec}

values for JD21 and Y-dyes are ~ 9 and ~ 16 Å, respectively (Table 3). The longer r_{rec}

distances in Y-dyes probably imply weaker recombination compared to JD21.

In the present work, the rates of injection and recombination were estimated by an

empirical model based on Marcus theory.[20] In this theory, the rate of nonadiabatic

electron transfer between two centers is calculated by:

$$k_{ET} = A\sqrt{\frac{\pi}{\hbar^2 \lambda k_B T}} \exp(-\beta r) \exp\left(\frac{-(-\Delta G^0 + \lambda)^2}{4k_B \lambda T}\right) \quad (1)$$

where, A is a constant (2.5×10^{-2}), $\hbar$ is the reduced Planck's constant, λ is the

reorganization energy in eV, k_B is Boltzmann constant, T is the room temperature

(289.15 K), β is attenuation factor (0.7 Å^{-1}), r is the distance of electron transfer in Å,

and ΔG^0 is the driving force of reaction in unit of eV.

The obtained values have been reported in Table 3. It turns out that Y-dyes show

evidently faster electron injection than the original JD21 dye. The rate of electron

injection (k_{inj}) is 1.83×10^{12}, 1.48×10^{12}, 5.84×10^{-2}, and 1.44×10^{-5} s^{-1} for Y1, Y2, Y3

and JD21, respectively. The faster injection for Y-dyes may efficiently decrease the

rapid decay of a dye from the excited state to the ground state. Different from the

obvious change of k_{inj} in the studied dyes, there exist smaller differences in the rates

of electron-hole recombination (k_{rec}). The Y3 dye with dithienopyrrole unit presents

the slowest recombination in all of dyes. The k_{rec} of dyes follows an order of Y3

$(9.38 \times 10^9 \text{ s}^{-1})$ < JD21 $(1.44 \times 10^{10} \text{ s}^{-1})$ < Y2 $(1.68 \times 10^{10} \text{ s}^{-1})$ < Y1 $(2.95 \times 10^{10} \text{ s}^{-1})$.

Compared with JD21, the faster electron injection and comparable electron-hole

recombination make the Y2 dye to be the champion molecule in kinetic processes. It

is also noted here that, although it is difficult to obtain accurate rates for injection and

recombination from this kind of estimation, it is conceivable that the comparison of

the rates obtained with the same model should give a useful indication to the

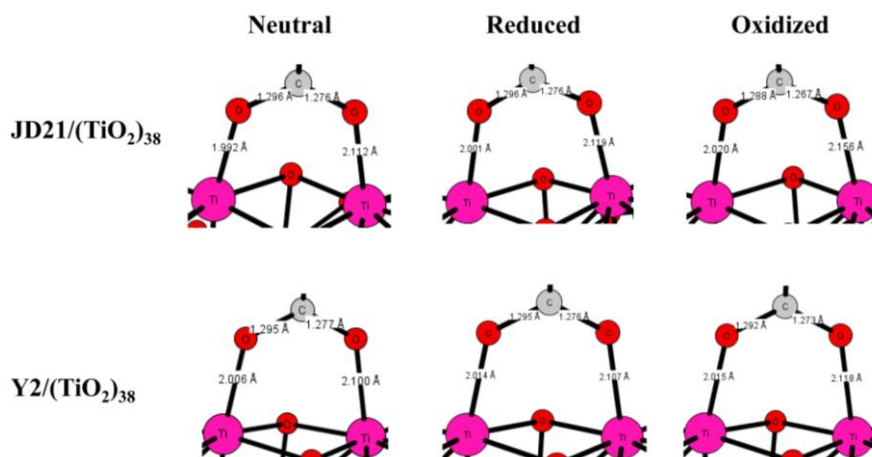performance of several similar dyes.

Figure 7. Structural details of the neutral, reduced, and oxidized dye/$(TiO_2)_{38}$

complexes.

3.2.4 Long-term stability of the adsorbed systems

One of the main reasons for the lack of long-term stability in DSC devices is the dye

desorption from the surface of semiconductor.[51] In current study, the stability of an

adsorbed system can be roughly assessed by its adsorption energy, i.e. the difference

between the energy of the optimized dye/$(TiO_2)_{38}$ complex and the energy sum of the

isolated fragments. Compared with JD21, the more negative adsorption energies in

Y-dyes (Table 2) may indicate the stronger interactions between Y-dyes and the

semiconductor surface. This can be further confirmed by the shorter bonds (within 2.0

~ 2.1 Å) between the carboxylic oxygens and the coordinating titanium atoms in the

oxidized Y-dye/$(TiO_2)_{38}$ complexes (Figures 7 and S12). These results may imply

higher stabilities of Y-dye/(TiO$_2$)$_{38}$ complexes relative to JD21.

With the comprehensive examinations described above, the newly-designed Y2 dye may be a promising candidate as DSC sensitizer. The solar cell sensitized by Y2 is expected to exhibit an improved DSC photovoltaic performance with a higher long-term stability.

4. Conclusion

In this paper, inspired by the successful utilization of silicon cores axially coordinated by trihexylsiloxy groups in naphthalo/phthalocyanine dyes, three novel silicon-core JD analogues were designed based on the JD21 backbone. A detailed theoretical investigation of the light-harvesting capability, thermodynamic property, kinetic parameter, and long-term stability of the corresponding dye/semiconductor complex has been performed to identify a potential good dye for DSC application. Our results highlight the significant influence of the silicon atom on the performance of a JD21-based dye. In particular, the Y2 dye with the dithienosilole (DTS) conjugation unit is identified to be a promising dye molecule, for its impressive performance in various aspects, including remarkable light-harvesting capability (the light-harvesting efficiency almost reach 100% in the range of 300-750 nm), large driving force for dye regeneration (ΔG_{reg} = 0.65 eV), excellent balance between the rates of electron injection (k_{inj} = 1.48$\times$10^{12} s^{-1}) and electron-hole recombination (k_{rec} = 1.68$\times$10^{10} s^{-1}), and high stability for the adsorbed system of Y2/(TiO$_2$)$_{38}$. Therefore, the solar cell sensitized by Y2 is expected to exhibit an improved DSC photovoltaic performance

with a higher long-term stability. The present study may provide a rational guide for experimental design of more efficient dyes for DSCs.

Acknowledgements

Table 1 The computed absorption wavelengths (λ), oscillator strengths (f), and the transition natures of dyes (H=HOMO, L=LUMO, etc.).

Dye	λ/nm	f	Main configurations	
JD21	522	1.16	H→L (97%)	
Y1	514	1.98	H→L (67%)	
	470[a]	0.04	H→L+1(76%)	
Y2	505	1.67	H→L (59%)	
	477[a]	0.10	H→L+1(73%)	
Y3	487	1.91	H→L (56%)	
	470[a]	0.19	H→L+1(69%)	
JD21/(TiO$_2$)$_{38}$	548	1.28	H→L+5 (28%)	H→L+6 (16%)
Y1/(TiO$_2$)$_{38}$	572	2.26	H→L+3 (22%)	H→L+2 (17%)
Y2/(TiO$_2$)$_{38}$	571	2.06	H→L+2 (35%)	H→L+1 (11%)
Y3/(TiO$_2$)$_{38}$	530	2.43	H→L+3 (27%)	H→L+4 (12%)

[a] The additional absorption bands of Y-dyes.

Table 2 The CB edge (E_{CB}, eV) of bare TiO_2, CB shift upon dye adsorption (ΔE_{CB}, eV), CB shift under addition of TBA^+ ion ($\Delta E_{CB\text{-}TBA}^+$, eV), charge transfer amount (CT, e^-), the average dye electrostatic potential (V_{EL}, eV) on the first layer of the TiO_2 surface, adsorption energy (E_{ads}, eV) for dyes adsorbed onto the $(TiO_2)_{38}$ cluster, and binding energy of the most stable dye-TBA^+ adducts (E_{bind}, eV).

Dye	E_{CB}/eV	ΔE_{CB}/eV	$\Delta E_{CB\text{-}TBA}^+$/eV	CT/e^-	V_{EL}/eV	E_{ads}/eV	E_{bind}/eV
JD21	-4.17	0.061	-0.055	0.49	-0.70	-1.15	-0.86
Y1	-4.17	0.046	-0.129	0.37	-6.20	-1.26	-0.78
Y2	-4.17	0.043	-0.135	0.50	-6.03	-1.23	—
Y3	-4.17	0.044	-0.134	0.54	-6.27	-1.23	—

Table 3 Driving forces, reorganization energies, charge transfer distances, injection and recombination rates estimated by Marcus theory.

Dye	GSOP/eV	E_{0-0}/eV	ESOP/eV	λ^{a}/eV	$\Delta G_{reg}{}^{b}$/eV	$\Delta G_{inj}{}^{c}$/eV	$\Delta G_{rec}{}^{d}$/eV	r_{inj}/Å	r_{rec}/Å	k_{inj}/s^{-1}	k_{rec}/s^{-1}
JD21	-5.29	2.51	-2.78	0.26	0.49	1.39	0.74	1.99	8.60	1.44×10^{-5}	1.44×10^{10}
Y1	-5.42	2.41	-3.01	0.51	0.62	1.16	0.86	2.00	16.07	1.83×10^{12}	2.95×10^{10}
Y2	-5.45	2.39	-3.05	0.48	0.65	1.12	0.89	2.00	15.39	1.48×10^{12}	1.68×10^{10}
Y3	-5.44	3.14	-2.30	0.48	0.64	1.87	0.88	2.00	16.46	5.84×10^{-2}	9.38×10^{9}

[a]The reorganization energy (λ) is assumed to be the same for both injection and recombination.

[b]Driving force for dye regeneration, $\Delta G_{reg} = \text{GSOP} - \mu(\text{I}^{-}/\text{I}_{3}^{-})$

[c]Driving force for electron injection, $\Delta G_{inj} = \text{ESOP} - E_{CB}$

[d]Driving force for electron-hole recombination, $\Delta G_{rec} = E_{CB} - \text{GSOP}$

References

1. B. E. Hardin, H. J. Snaith and M. D. McGehee, *Nat. Photon.*, 2012, 6, 162-169.

2. M. F. Xu, M. Zhang, M. Pastore, R. Z. Li, F. De Angelis and P. Wang, *Chem. Sci.*, 2012, 3, 976-983.

3. A. K. Chandiran, M. Abdi-Jalebi, M. K. Nazeeruddin and M. Grätzel, *ACS Nano*, 2014, 8, 2261-2268.

4. B. O'Regan and M. Grätzel, *Nature*, 1991, 353, 737-740.

5. A. Yella, H.-W. Lee, H. N. Tsao, C. Yi, A. K. Chandiran, M. K. Nazeeruddin, E. W.-G. Diau, C.-Y. Yeh, S. M. Zakeeruddin and M. Grätzel, *Science*, 2011, 334, 629-634.

6. A. Maufroy, L. Favereau, F. B. Anne, Y. Pellegrin, E. Blart, M. Hissler, D. Jacquemin and F. Odobel, *J. Mater. Chem. A*, 2015, 3, 3908-3917.

7. T. Kinoshita, J. T. Dy, S. Uchida, T. Kubo and H. Segawa, *Nat. Photon.*, 2013, 7, 535-539.

8. C. C. Chou, F. C. Hu, H. H. Yeh, H. P. Wu, Y. Chi, J. N. Clifford, E. Palomares, S. H. Liu, P. T. Chou and G. H. Lee, *Angew. Chem. Int. Ed.*, 2014, 53, 178-183.

9. J. Luo, M. Xu, R. Li, K. W. Huang, C. Jiang, Q. Qi, W. Zeng, J. Zhang, C. Chi, P. Wang and J. Wu, *J. Am. Chem. Soc.*, 2014, 136, 265-272.

10. S.-L. Chen, L.-N. Yang and Z.-S. Li, *J. Power Sources*, 2013, 223, 86-93.

11. J.-Z. Zhang, J. Zhang, H.-B. Li, Y. Wu, H.-L. Xu, M. Zhang, Y. Geng and Z.-M. Su, *J. Power Sources*, 2014, 267, 300-308.

12. G. Tian, S. Cai, X. Li, H. Agren, Q. Wang, J. Huang and J. Su, *J. Mater. Chem. A*, 2015, 3, 3777-3784.

13. J. Yang, P. Ganesan, J. Teuscher, T. Moehl, Y. J. Kim, C. Yi, P. Comte, K. Pei, T. W. Holcombe, M. K. Nazeeruddin, J. Hua, S. M. Zakeeruddin, H. Tian and M. Grätzel, *J. Am. Chem. Soc.*, 2014, 136, 5722-5730.

14. D. Casanova, *ChemPhysChem*, 2011, 12, 2979-2988.

15. S. Meng, E. Kaxiras, M. K. Nazeeruddin and M. Grätzel, *J. Phys. Chem. C*, 2011, 115, 9276-9282.

16. L.-N. Yang, Z.-Z. Sun, S.-L. Chen and Z.-S. Li, *Dyes Pigm.*, 2013, 99, 29-35.

17. K. Kakiage, Y. Aoyama, T. Yano, T. Otsuka, T. Kyomen, M. Unno and M. Hanaya, *Chem. Commun.*, 2014, 50, 6379-6381.

18. K. Kakiage, T. Tokutome, S. Iwamoto, T. Kyomen and M. Hanaya, *Chem. Commun.*, 2013, 49, 179-180.

19. J. H. Delcamp, A. Yella, T. W. Holcombe, M. K. Nazeeruddin and M. Grätzel, *Angew. Chem. Int. Ed.*, 2013, 52, 376-380.

20. W. Ma, Y. Jiao and S. Meng, *J. Phys. Chem. C*, 2014, 118, 16447-16457.

21. J. Feng, Y. Jiao, W. Ma, M. K. Nazeeruddin, M. Grätzel and S. Meng, *J. Phys. Chem. C*, 2013, 117, 3772-3778.

22. B. Lim, G. Y. Margulis, J.-H. Yum, E. L. Unger, B. E. Hardin, M. Grätzel, M. D. McGehee and A. Sellinger, *Org. Lett.*, 2013, 15, 784-787.

23. J. Liu, X. Yang and L. Sun, *Chem. Commun.*, 2013, 49, 11785-11787.

24. M. Zhang, Y. Wang, M. Xu, W. Ma, R. Li and P. Wang, *Energy Environ. Sci.*, 2013, 6, 2944-2949.

25. J. Zhang, Z. Yao, Y. Cai, L. Yang, M. Xu, R. Li, M. Zhang, X. Dong and P. Wang, *Energy Environ.*

Sci., 2013, 6, 1604-1614.

26.   W. Zeng, Y. Cao, Y. Bai, Y. Wang, Y. Shi, M. Zhang, F. Wang, C. Pan and P. Wang, *Chem. Mater.*, 2010, 22, 1915-1925.

27.   N. Cai, J. Zhang, M. Xu, M. Zhang and P. Wang, *Adv. Funct. Mater.*, 2013, 23, 3539-3547.

28.   A. D. Becke, *J. Chem. Phys.*, 1993, 98, 5648-5652.

29.   M. Cossi, N. Rega, G. Scalmani and V. Barone, *J. Comput. Chem.*, 2003, 24, 669-681.

30.   T. Yanai, D. P. Tew and N. C. Handy, *Chem. Phys. Lett.*, 2004, 393, 51-57.

31.   L.-N. Yang, Z.-Z. Sun, Q.-S. Li, S.-L. Chen, Z.-S. Li and T. A. Niehaus, *J. Power Sources*, 2014, 268, 137-145.

32.   M.J. Frisch, G.W. Trucks, H.B. Schlegel, G.E. Scuseria, M.A. Robb, J.R. Cheeseman, G. Scalmani, V. Barone, B. Mennucci, G. A. Petersson, H. Nakatsuji, M. Caricato, X. Li, H.P. Hratchian, A.F. Izmaylov, J. Bloino, G. Zheng, J.L. Sonnenberg, M. Hada, M. Ehara, K. Toyota, R. Fukuda, J. Hasegawa, M. Ishida, T. Nakajima, Y. Honda, O. Kitao, H. Nakai, T. Vreven, J.A. Montgomery, J. E. P. Jr., F. Ogliaro, M. Bearpark, J.J. Heyd, E. Brothers, K.N. Kudin, V.N. Staroverov, R. Kobayashi, J. Normand, K. Raghavachari, A. Rendell, J.C. Burant, S.S. Iyengar, J. Tomasi, M. Cossi, N. Rega, J.M. Millam, M. Klene, J.E. Knox, J.B. Cross, V. Bakken, C. Adamo, J. Jaramillo, R. Gomperts, R.E. Stratmann, O. Yazyev, A.J. Austin, R. Cammi, C. Pomelli, J.W. Ochterski, R.L. Martin, K. Morokuma, V.G. Zakrzewski, G.A. Voth, P. Salvador, J.J. Dannenberg, S. Dapprich, A.D. Daniels, O. Farkas, J.B. Foresman, J.V. Ortiz, J. Cioslowski and D.J. Fox, *Gaussian 09. Revision B.01. Wallingford CT: Gaussian Inc.;*, 2009.

33.   F. De Angelis, C. Di Valentin, S. Fantacci, A. Vittadini and A. Selloni, *Chem. Rev.*, 2014, 114, 9708-9753.

34.   M. Lazzeri, A. Vittadini and A. Selloni, *Phys. Rev. B*, 2001, 63, 155409.

35.   M. Lazzeri, A. Vittadini and A. Selloni, *Phys. Rev. B*, 2002, 65, 119901.

36.   J. P. Perdew, K. Burke and M. Ernzerhof, *Phys. Rev. Lett.*, 1996, 77, 3865-3868.

37.   J. P. Perdew, K. Burke and M. Ernzerhof, *Phys. Rev. Lett.*, 1997, 78, 1396-1396.

38.   A. Klamt and G. Schuurmann, *J. Chem. Soc., Perkin Trans. 2*, 1993, 799-805.

39.   B. Delley, *J. Chem. Phys.*, 1990, 92, 508-517.

40.   B. Delley, *J. Chem. Phys.*, 2000, 113, 7756-7764.

41.   E. Ronca, M. Pastore, L. Belpassi, F. Tarantelli and F. De Angelis, *Energy Environ. Sci.*, 2013, 6, 183-193.

42.   L. Belpassi, I. Infante, F. Tarantelli and L. Visscher, *J. Am. Chem. Soc.*, 2007, 130, 1048-1060.

43.   S. Taya, S. Kuwahara, Q. Shen, T. Toyoda and K. Katayama, *RSC Adv.*, 2014, 4, 21517-21520.

44.   T. Le Bahers, F. Labat, T. Pauporte, P. P. Laine and I. Ciofini, *J. Am. Chem. Soc.*, 2011, 133, 8005-8013.

45.   T. Le Bahers, F. Labat, T. Pauporte and I. Ciofini, *Phys. Chem. Chem. Phys.*, 2010, 12, 14710-14719.

46.   S. Agrawal, T. Leijtens, E. Ronca, M. Pastore, H. Snaith and F. De Angelis, *J. Mater. Chem. A*, 2013, 1, 14675-14685.

47.   S. Fantacci, M. G. Lobello and F. De Angelis, *Chimia (Aarau)*, 2013, 67, 121-128.

48.   F. d. r. Labat, I. Ciofini, H. P. Hratchian, M. J. Frisch, K. Raghavachari and C. Adamo, *J. Phys. Chem. C*, 2011, 115, 4297-4306.

49.   T. Le Bahers, T. Pauporté, P. P. Lainé, F. Labat, C. Adamo and I. Ciofini, *J. Phys. Chem. Lett.*, 2013, 4, 1044-1050.

50.   A. Yella, R. Humphry-Baker, B. F. E. Curchod, N. Ashari Astani, J. Teuscher, L. E. Polander, S. Mathew, J.-E. Moser, I. Tavernelli, U. Rothlisberger, M. Grätzel, M. K. Nazeeruddin and J. Frey, *Chem. Mater.*, 2013, 25, 2733-2739.

51.   P. Salvatori, S. Agrawal, C. Barreddi, C. Malapaka, M. de Borniol and F. De Angelis, *RSC Adv.*, 2014, 4, 57620-57628.